RSC Advances

PAPER

View Article Online
View Journal | View Issue

Cite this: *RSC Adv.*, 2021, **11**, 22278

Copper nanoparticle anchored biguanidine-modified Zr-UiO-66 MOFs: a competent heterogeneous and reusable nanocatalyst in Buchwald–Hartwig and Ullmann type coupling reactions†

Hojat Veisi,*[a] Narges Neyestani,[a] Mozhgan Pirhayati,[b] Sheida Ahany Kamangar,[a] Shahram Lotfi,[a] Taiebeh Tamoradi*[c] and Bikash Karmakar*[d]

Received 3rd April 2021
Accepted 18th June 2021

DOI: 10.1039/d1ra02634h

rsc.li/rsc-advances

We have designed a functionalized metal–organic framework (MOF) of UiO topology as a support, with an extremely high surface area, adjustable pore sizes and stable crystalline coordination polymeric structure and implanted copper (Cu) nanoparticles thereon. The core three dimensional Zr-derived MOF (UiO-66-NH_2) was modified with a biguanidine moiety following a covalent post-functionalization approach. The morphological and physicochemical features of the material were determined using analytical methods such as FT-IR, SEM, TEM, EDX, atomic mapping, XRD and ICP-OES. The SEM and XRD results justified the unaffected morphology of Zr-MOF after structural modifications. The as-synthesized UiO-66-biguanidine/Cu nanocomposite was catalytically explored in the aryl and heteroaryl Buchwald–Hartwig C–N and Ullmann type C–O cross coupling reactions with excellent yields. A library of biaryl amine and biaryl ethers was synthesized over the catalyst under mild and green conditions. Furthermore, the catalyst was isolated by centrifugation and recycled 11 times with no significant copper leaching or change in its activity.

1. Introduction

The transition metals (TMs) possess great affinity to form a broad range of complexes with various organic ligands based on their incompletely filled atomic orbitals. There are many reports of transition metal complexes in chelation with synthetically designed and suitably oriented novel organic ligands, which have otherwise numerous applications as homogeneous catalysts in different organic transformations.[1–5] However, the catalyst isolation and reusability have been the major issue that restricts their use in view of eco-sustainability. Thereby, heterogenization of the TM complexes by immobilization over different solid supports like silica,[6] magnetic nanoparticles,[7] carbon nanotubes,[8] mesoporous silica,[9] zeolites[10] and layered materials[11] has been extensively explored in view of easy handling, thermal stability, facile isolation and reusability.[12] Still, there remain problems like non-uniform distribution of catalysts and difficulty in characterizing such entities.[13] This has prompted us to design functionalized metal–organic frameworks (MOFs) and subsequently anchor appropriate active sites into it. In the last few years MOFs have been come out as a significant group of porous materials having huge surface areas, high degree of tunability in terms of shape and dimensions of pore channels and pore sizes, defined and diverse crystal structures, uniformly distributed active sites in the whole network, adjustable active metal concentration and possess high compatibility in chemical functionalizations towards the secondary active metal chelations.[14–16] Due to such unique features, different engineered MOFs find potential applications in separation, drug delivery, magnetism, gas storage, adsorption, water treatment, health-care applications, chemical sensing, non-linear optics, and as a nano reactor in catalysis.[17–20] In this context, we wish to introduce a novel MOF based heterogeneous catalytic system, the Cu adorned biguanidine functionalized UiO-66-NH_2 (UiO-66-biguanidine/Cu). The core skeleton is being synthesized with $[Zr_6O_4(OH)_4]$ octahedral secondary building units (SBU) and 2-amino-1,4-benzene dicarboxylate (BDC) ligands where each Zr_6 cluster is three dimensionally coordinated to 12 BDC units forming a hierarchical framework.[21–24] The biguanidine functionality, which is

[a]Department of Chemistry, Payame Noor University (PNU), Tehran, Iran. E-mail: hojatveisi@yahoo.com
[b]Department of Applied Chemistry, Faculty of Science, Malayer University, Malayer, Iran
[c]Chemistry Department, Production Technology Research Institute-ACECR, Ahvaz, Iran. E-mail: t.tabss@yahoo.com
[d]Department of Chemistry, Gobardanga Hindu College, 24-Parganas (North), India. E-mail: bkarmakar@ghcollege.ac.in

† Electronic supplementary information (ESI) available. See DOI: 10.1039/d1ra02634h

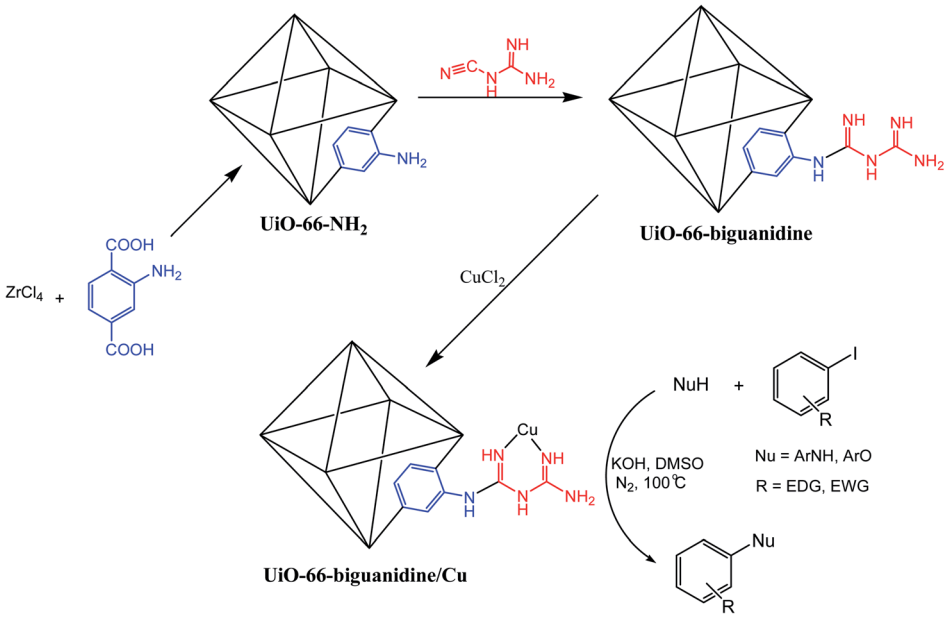

Scheme 1 Schematic designing of UiO-66-biguanidine/Cu nanocomposite and its application in the C-heteroatom coupling reactions.

known to be an excellent chelating ligand, has been post-immobilized over it and subsequently Cu NPs have been anchored thereon as the active catalytic site (Scheme 1). In synthetic organic chemistry there are limited catalytic applications of post-synthetic modified MOFs *via* covalent surface functionalization with homodispersed co-operative active

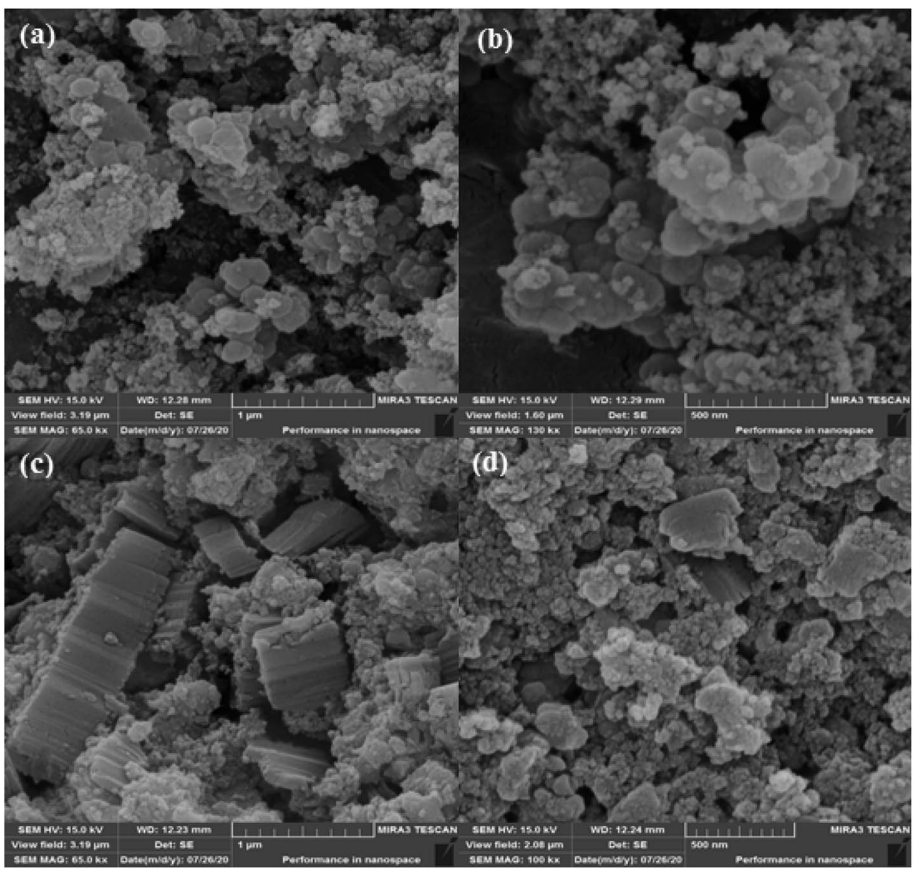

Fig. 1 SEM images of UiO-66-NH_2 (a and b); and UiO-66-biguanidine/Cu nanocomposite (c and d).

sites.[25–29] Being encouraged by this and also in continuation to our ongoing endeavors on the development and synthetic utilizations of architectured heterogeneous nanocatalysts,[30–38] we report the catalytic application of UiO-66-biguanidine/Cu in efficient C–N and C–O heterocoupling reactions (Scheme 1). These coupled products, especially those involving heterocycles, find extensive applications as important drugs and medicines, materials and also in biology.[39–41] Earlier, a number of research groups have reported the C-heteroatom cross coupling reactions over Cu catalysts.[42–48] However, most of the protocols involved various ligand based homogeneous catalysts or heterogeneous catalysts being synthesized using toxic and strong reducing agents. The procedure devised by us using UiO-66-biguanidine/Cu catalyst is the first report for an efficient, ligand free green synthesis of C-heteroatom coupled products with outstanding yields in quick intervals, making the overall procedure industrially and sustainably viable.

2. Experimental

2.1 Synthesis of UiO-66-NH_2

1.166 g $ZrCl_4$ (5 mmol) was dissolved in 2 mL DMF in presence of HCl (5 mL) under sonication for 20 min at ambient conditions. A solution of 2-aminobenzene-1,4-dicarboxylic acid (5 mmol, 0.9057 g) in DMF (30 mL) was then mixed to it and sonicated again for 20 min. The whole mixture was warmed at 80 °C for 6 h followed by heating at 100 °C for 24 h. On cooling the product was obtained as microcrystalline powder. It was isolated by centrifugation at 4000 rpm for 20 min and then washed thrice with DMF and EtOH (30 mL). Finally, UiO-66-NH_2 was obtained as yellow powder (95%) on drying under vacuum at 100 °C for 24 h.

2.2 Synthesis of UiO-66-biguanidine

A 50 mL aqueous dispersion containing 0.5 g of UiO-66-NH_2 was sonicated for 10 min and then an HCl solution (0.15 mol L^{-1}, 50 mL) of 0.168 g dicyandiamide (2 mmol) was added to it. The mixture was heated at 100 °C for 24 h. It was cooled and worked up with 10% NaOH solution which resulted the UiO-66-biguanidine. The solid was collected by centrifugation at 4000 rpm for 20 min. It was washed thoroughly with 1 : 1 EtOH and dried as before.

2.3 Synthesis of UiO-66-biguanidine/Cu

0.5 g of UiO-66-biguanidine was sonicated well in H_2O (50 mL) until a homogenous dispersion was obtained. Then an aqueous solution of $CuCl_2$ (50 mL, 1 mg mL^{-1}) was mixed to it as Cu source and the mixture was triturated at 12 h. The product was isolated by centrifuger and washed twice with 20 mL water followed by with 20 mL ethanol. It was dried under vacuum at 60 °C for 24 h. Cu content in UiO-66-biguanidine/Cu was found as 0.31 mmol g^{-1} by ICP-OES analysis.

2.4 UiO-66-biguanidine/Cu catalyzed C–N and C–O coupling

A mixture of N/O nucleophile (1 mmol), aryl halide (1.1 mmol) and KOH (1.5 mmol) were taken together in 3 mL dry DMF in presence of 0.8 mol% UiO-66-biguanidine/Cu catalyst at 100 °C under N_2 atmosphere for requisite times. On completion (monitored by TLC), the reaction was brought to ambient conditions and the catalyst was separated by centrifugation. The reaction was worked up in 10 mL water and the product was extracted into EtOAc. The organic layer was washed with brine-water (10 mL), dried over Na_2SO_4, concentrated and finally purified by silica gel column chromatography.

3. Results and discussions

3.1 Catalyst characterization data analysis

On complete synthesis of the material following post-functionalization, we turned our attention to evaluate its structural and physicochemical characteristics using several analytical techniques like FT-IR, SEM, TEM, EDX, elemental mapping and XRD. Fig. S1† displays the comparative FT-IR spectra of UiO-66-NH_2, UiO-66-biguanidine and UiO-66-biguanidine/Cu in order to understand the stepwise building of the material. In the spectrum of UiO-66-NH_2 (Fig. S1a†), typical vibrations appeared at 1405 and 1571 cm^{-1} can be credited to the symmetric and asymmetric stretching vibrations of carboxylate groups from BDC. The H–N–H scissoring and the C–NH_2 stretching vibrations of aromatic amines are observed at

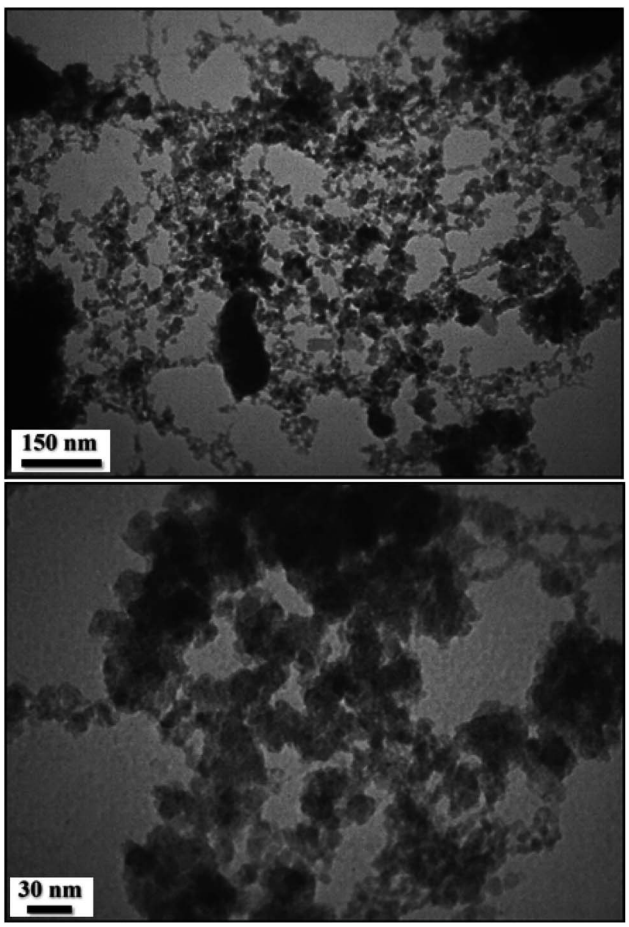

Fig. 2 TEM images of UiO-66-NH_2.

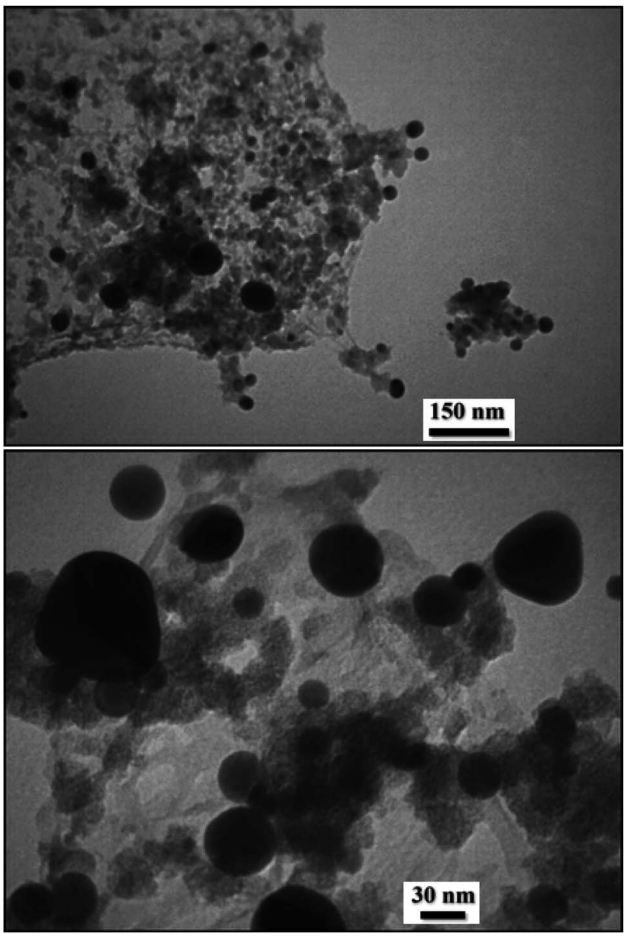

Fig. 3 TEM images of UiO-66-biguanidine/Cu nanocomposite.

1259 cm^{-1} and 1658 cm^{-1} respectively. The broad peaks at 3381 cm^{-1} and 3503 cm^{-1} are due to the N–H symmetric and asymmetric stretching vibrations respectively. On reaction of UiO-66-NH_2 with dicyandiamide, it results the biguanidine/UiO-66 moiety, which was confirmed from the disappearance of all the free amine related peaks (1658, 3381, 3503 cm^{-1}) while all other peaks remained unchanged (Fig. S1b†). However, no significant changes are observed in the spectrum of UiO-66-biguanidine/Cu from Fig. 1b, as the characteristic bands due to immobilization Cu on the biguanidine/Zr-MOF are very weak to be distinguished (Fig. S1c†).

The particle size, shape and texture of UiO-66-NH_2 and UiO-66-biguanidine/Cu was explored over SEM and represented in Fig. 1 at different magnifications. Both the samples have typical structure consisting of irregular intergrown microcrystalline polyhedra with a mean diameter of 50 to 90 nm. In a cross-sectional view, stacking units can be observed in Fig. 1c. No significant change in morphology is observed in the structure on post-functionalization or Cu attachment over it. The particles seem to be somewhat agglomerated due to high concentration during sample preparations.

Further justification of SEM investigation towards the detailed structural inherence regarding size and morphology was carried out through TEM analysis of the UiO-66-NH_2 (Fig. 2) and UiO-66-biguanidine/Cu nanocomposite (Fig. 3). With comparison of these images, successful formation and immobilization of the copper monodispersed spherical shaped nanoparticles with a mean diameter of 20–40 nm could be confirmed in the Fig. 3. On close observation, stacking structural units of MOF can be observed.

The chemical constitutions of both UiO-66-NH_2 and UiO-66-biguanidine/Cu nanocomposite were established on EDX detector equipped with SEM instrument and represented in Fig. 4. The EDX spectrum of UiO-66-NH_2 showed the peaks of Zr, C, N and O atoms which narrate the structural components being Zr as SBU and C, N, O signifying the BDC ligand (Fig. 4a). Fig. 4b exhibits the EDX profile of UiO-66-biguanidine/Cu, where it shows the Cu as element in addition to the previous elements signifying the attachment of Cu nanoparticles to UiO-66-biguanidine, a derivative of UiO-66-NH_2.

The EDX data was further justified through X-ray atomic mapping and demonstrated in Fig. 5. Additionally, it shows the distribution of the constitutional elements in UiO-66-biguanidine/Cu nanocomposite. An X-ray sectional scanning of the surface displays the homogeneous dispersion of Zr, C, N and Cu atoms over the surface. Obviously, Zr and C display much higher density than other elements, as being the core component of the motif. The uniformity of active component definitely reasons for its excellent catalytic performances.

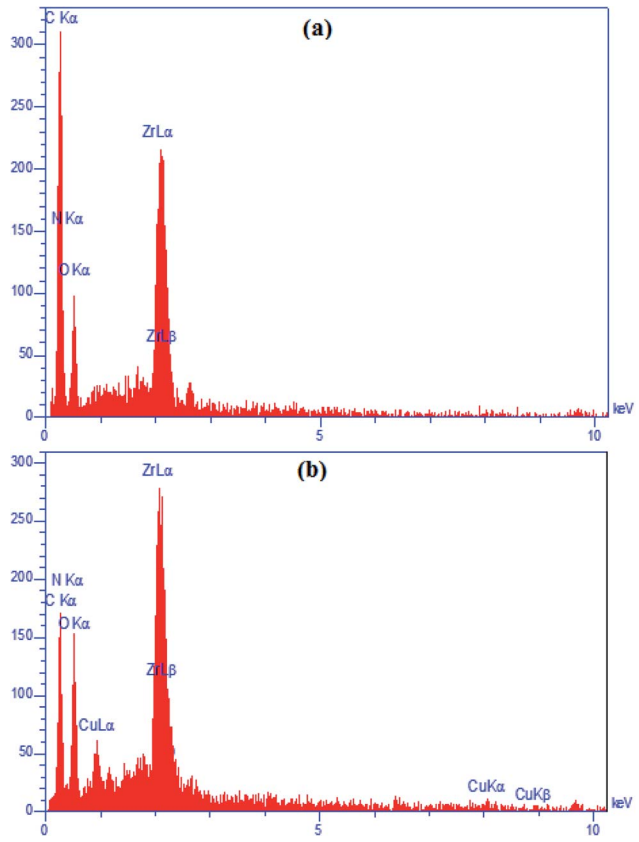

Fig. 4 EDX spectra of UiO-66-NH_2 (a); and Cu@bigua/UiO-66 nanocomposite (b).

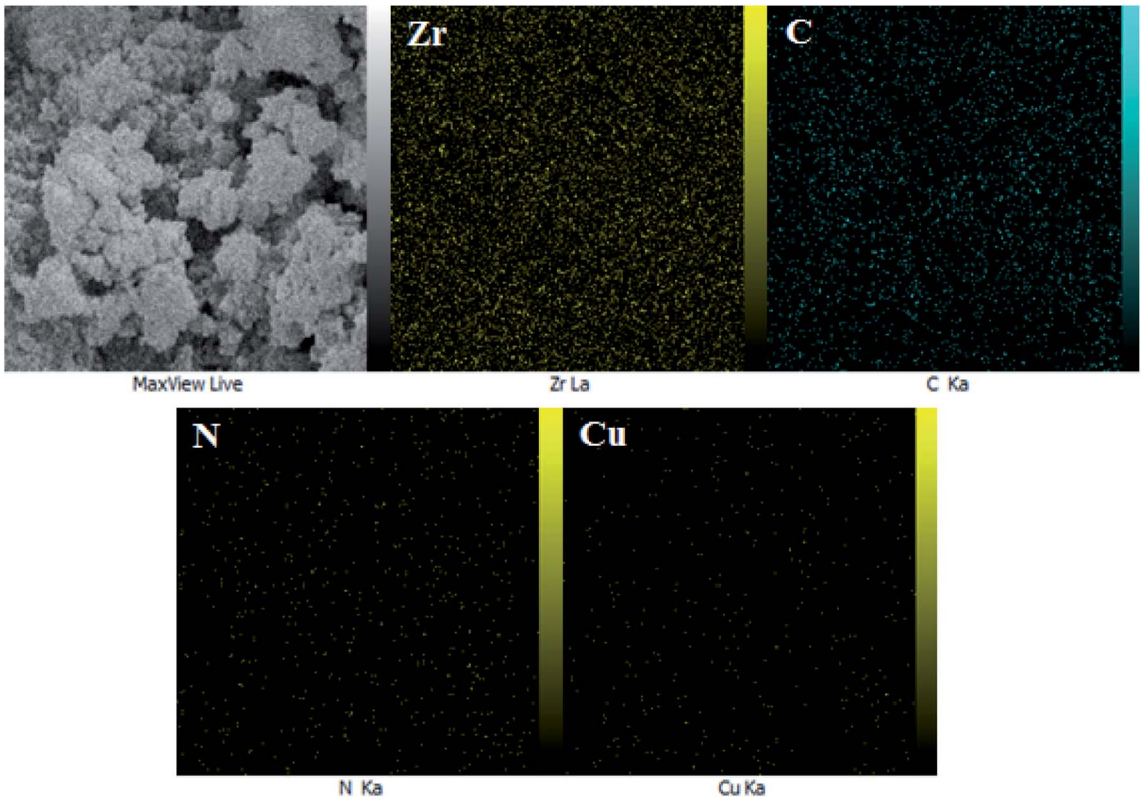

Fig. 5 Elemental mapping of UiO-66-biguanidine/Cu nanocomposite.

Table 1 Nitrogen adsorption–desorption data for UiO-66-NH_2, UiO-66-biguanidine and UiO-66-biguanidine/Cu

Entry	Samples	S_{BET} ($m^2\ g^{-1}$)	Total pore volume ($cm^3\ g^{-1}$)	Mean pore diameter (nm)
1	UiO-66-NH_2	1045	0.68	0.62
2	UiO-66-biguanidine	923	0.42	0.58
3	UiO-66-biguanidine/Cu	810	0.22	0.53

The nitrogen adsorption–desorption isotherms of UiO-66-NH_2, UiO-66-biguanidine and UiO-66-biguanidine/Cu are studied and the corresponding data are summarized in Table 1. It can be seen that the structures of each sample featured the type I isotherm. The Langmuir surface area of the UiO-66-NH_2 was 1045 $m^2\ g^{-1}$ with pore volume of 0.68 $cm^3\ g^{-1}$. After the biguanidine modification, the Langmuir surface area decreased to 923 $m^2\ g^{-1}$, while the pore volume decreased to 0.42 $cm^3\ g^{-1}$, which indicates occupation of the internal channels by biguanidine moieties in Zr-MOF structure.[49] The Langmuir surface area of UiO-66-biguanidine/Cu catalyst decreases to 810 $m^2\ g^{-1}$ when the copper moiety is introduced.

The crystallinity and phase structure of UiO-66-NH_2 and UiO-66-biguanidine/Cu nanocomposite were analyzed by XRD study (Fig. 6). Evidently, both the materials are poorly crystalline in nature. Three significant Braggs diffraction peaks of the UiO-66-NH_2 are observed at $2\theta = 7.32$, 8.72 and 25.93° respectively, which are in close agreement with the literature. The UiO-66-biguanidine/Cu exhibits almost similar XRD pattern as the basic UiO-66-NH_2 material, which indicates the unaltered framework even after surface modifications. There was no significant peak of Cu detected in the profile.

3.2 Catalytic applications of UiO-66-biguanidine/Cu nanocomposite

After the complete characterizations of the as-synthesized final material, we paid attention on the catalytic applications. We inspected the performance of UiO-66-biguanidine/Cu nanocomposite in the Buchwald–Hartwig (C–N) and Ullmann (C–O) type coupling reactions. Several iodobenzene derivatives were coupled to various N and O nucleophiles in presence of an additive base over our catalyst, following a simplistic clean protocol. After completion, the catalyst was retrieved by centrifuge and recycled in consecutive runs. However, prior to general studies, optimization of the reaction conditions seemed quite significant and hence, a reaction between indole and

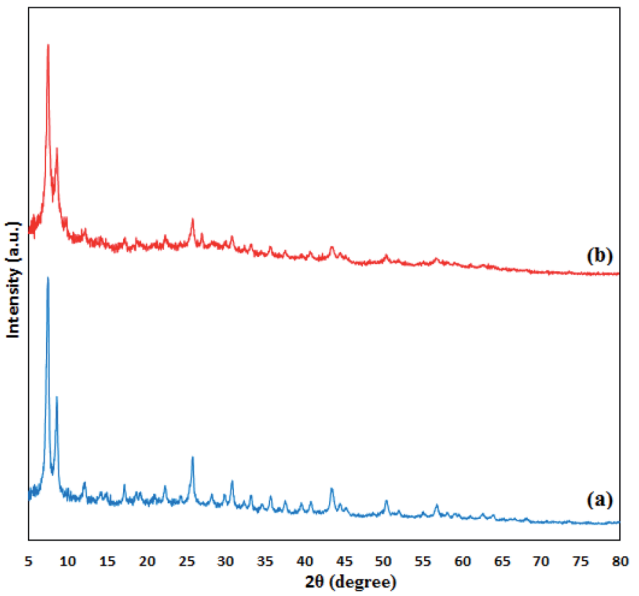

Fig. 6 XRD patterns of UiO-66-NH_2 (a); and UiO-66-biguanidine/Cu nanocomposite (b).

iodobenzene was selected as a model and an array of screening experiments were conducted applying diverse conditions like catalyst load, solvent, base and temperature. The outcomes are shown in Table 2. In the absence of catalyst, there was absolutely no product at all and a poor yield was obtained in the lack of external base, which signifies their importance in the reaction (Table 2, entries 10 and 11). In presence of catalyst and a base, the reaction yield gradually increases and we got the best output over 0.8 mol% Cu loaded catalyst and KOH as base at 100 °C in DMF solvent (Table 2, entry 8). A moderate yield was obtained at lower temperatures (Table 2, entries 5 and 6). While screening the reaction in different solvents like EtOH, DMF, toluene, DMSO, CH_2Cl_2 and CH_3CN, we got the best result in DMF (Table 2, entries 1–6). As the external base was significant in the reaction, we also studied the influence of various bases like KOH, $NaHCO_3$, Et_3N, Na_2CO_3 and K_2CO_3, when the first one afforded the best yield while the others resulted moderate to good yields (entries 8–14). Optimizing the reaction conditions with N-nucleophile, the same were applied using phenol as an O-nucleophile in the reaction which also produced 90% yield. This justifies the authenticity of the said stabilized conditions. Additionally, we carried out the variation of catalysts with the stabilized conditions over the probe reaction which has been shown separately in Table 3. Different precursors and intermediates of the final catalyst were involved in the catalysis in

Table 3 Variation of catalysts in the cross coupling of indole with iodobenzene[a]

Entry	Catalyst	Time (h)	Yield[b] (%)
1	UiO-66	24	0
2	UiO-66-biguanidine	24	0
3	UiO-66-Cu	10	72
4	UiO-66-biguanidine/Cu	10	96

[a] Reaction conditions: indole (1.0 mmol), iodobenzene (1.1 mmol), KOH (1.5 mmol), DMF (3.0 mL), 100 °C, N_2 atmosphere. [b] Isolated yield.

Table 2 Optimization of reaction condition for UiO-66-biguanidine/Cu catalyzed cross coupling of indole/phenol with iodobenzene[a]

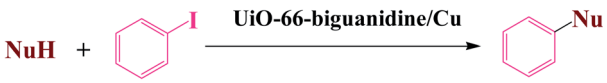

Entry	NuH	Cat. (mol%)	Base	Solvent	T (°C)	t (h)	Yield[b] (%)
1	Indole	0.3	KOH	EtOH	80	10	55
2	Indole	0.3	KOH	DMF	100	10	75
3	Indole	0.3	KOH	Toluene	100	10	65
4	Indole	0.3	KOH	DMSO	100	10	65
5	Indole	0.3	KOH	CH_2Cl_2	60	24	40
6	Indole	0.3	KOH	CH_3CN	70	24	50
7	Indole	0.6	KOH	DMF	100	10	90
8	**Indole**	**0.8**	**KOH**	**DMF**	**100**	**10**	**96**
9	Indole	0.8	—	DMF	100	24	Trace
10	Indole	—	KOH	DMF	100	24	0
11	Indole	0.8	K_2CO_3	DMF	100	12	75
12	Indole	0.8	Na_2CO_3	DMF	100	12	60
13	Indole	0.8	Et_3N	DMF	100	10	85
14	Indole	0.8	$NaHCO_3$	DMF	100	10	60
15	Indole	0.8	KOH	DMF	80	10	75
16	Indole	0.8	KOH	DMF	25	10	30
17	Phenol	0.8	KOH	DMF	100	10	90

[a] Reaction conditions: N/O nucleophile (1.0 mmol), iodobenzene (1.1 mmol), UiO-66-biguanidine/Cu, base (1.5 mmol), solvent (3.0 mL), N_2 atmosphere. [b] Isolated yield.

order to identify and investigate the role of active site. The reaction was absolutely failed over UiO-66 and UiO-biguanidine as catalyst which indicates there is definitely a role of Cu in the reaction. Now, to get a deeper insight we involved the Cu(II) impregnated UiO-66 (UiO-66/Cu) composite in the reaction where it afforded a moderate 72% yield. This result is very interesting signifying the role of biguanidine, which has an important role in stabilizing the Cu NP and also to prevent the metal to leach. Moreover, biguanidine also protects the Cu NPs to agglomerate.

On stabilizing the optimum conditions, the investigations were extended in search for their generalizations through substrate variations. A wide range of biaryl amine and biaryl ether derivatives were synthesized by coupling of diverse aryl iodides and aryl/heteroaryl amines or phenols under the optimized conditions (Table 4). Among the N-nucleophiles (Table 4, entries 1–15), aniline reacted much faster (4–5 h) as compared to indole or imidazole (10–12 h) towards the N-coupled products, whereas, the aryl iodides were highly reactive irrespective of their substitutions, being electron donating (CH_3, OCH_3) or electron withdrawing (NO_2). In most of the cases excellent yields were obtained (>90%). Similarly, different phenols and their derivatives were also equally compatible with various aryl iodides resulting very good productivity (entries 16–24). All the products are known, as given in the references, being justified from ^{1}H NMR data.

Table 4 UiO-66-biguanidine/Cu catalyzed coupling of amines and phenols with aryl iodides[a]

Entry	Substrate	Aryl iodide	Time (h)	Yield[b] (%)	Ref.[c]
1	Indole	C_6H_5I	10	96	50
2	Indole	*p*-$CH_3C_6H_4I$	10	95	51
3	Indole	*p*-ClC_6H_4I	10	95	50
4	Indole	*p*-$CH_3OC_6H_4I$	10	90	50
5	Indole	*p*-$NO_2C_6H_4I$	10	92	50
6	Indole	*o*-$CH_3OC_6H_4I$	12	90	50
7	Aniline	C_6H_5I	5	96	52
8	Aniline	*p*-$CH_3C_6H_4I$	4	95	53
9	Aniline	*p*-ClC_6H_4I	5	90	53
10	Aniline	*p*-$CH_3OC_6H_4I$	5	90	54
11	Aniline	*p*-$NO_2C_6H_4I$	4	95	52
12	Aniline	*o*-$CH_3OC_6H_4I$	5	90	55
13	Imidazole	C_6H_5I	12	88	53
14	Imidazole	*p*-$CH_3C_6H_4I$	12	85	56
15	Imidazole	*p*-$CH_3OC_6H_4I$	12	70	57
16	Pyrrole	C_6H_5I	10	91	53
17	Benzimidazole	C_6H_5I	12	86	53
18	Phenol	C_6H_5I	10	90	58
19	Phenol	*p*-$CH_3C_6H_4I$	10	90	59
20	Phenol	*p*-ClC_6H_4I	10	88	55
21	Phenol	*p*-$CH_3OC_6H_4I$	10	92	55
22	Phenol	*p*-$NO_2C_6H_4I$	8	92	55
23	Phenol	*o*-$CH_3OC_6H_4I$	12	75	60
24	4-Methylphenol	C_6H_5I	12	80	60
25	4-Methoxylphenol	C_6H_5I	12	92	60
26	2-Methylphenol	C_6H_5I	24	85	60

[a] Reaction conditions: amines/phenols (1.0 mmol), iodobenzene (1.1 mmol), UiO-66-biguanidine/Cu (0.8 mol%), KOH (1.5 mmol), DMF (3.0 mL), stirring, nitrogen atmosphere, 100 °C. [b] Isolated yield. [c] Known product.

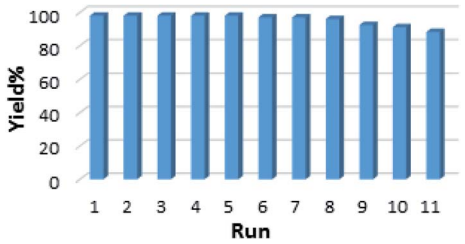

Fig. 7 Recycling of the UiO-66-biguanidine/Cu nanocomposite catalyst in the reaction between indole with iodobenzene.

3.3 Reusability study of catalyst

In order to validate the catalytic sustainability and green chemical methodology, the study of reusability is an utmost important criterion. After completion of the fresh cycle of the reaction between indole and iodobenzene, the catalyst was recollected by centrifuger and thoroughly washed with aqueous EtOH. It was regenerated by drying and used in the successive runs. The UiO-66-biguanidine/Cu nanocomposite showed significant reactivity upto 11 successive cycles with only a nominal change in yields. The yield was slightly decreased after 8th run probably due to agglomeration of catalysts. The outcome has been displayed in Fig. 7. Also the ICP-AES analysis of the catalyst after 8 runs was shown that amount of Cu loaded on the catalyst is 0.30 mmol g^{-1}, that was shown a slight change in amount of Cu (0.31 to 0.30 mmol g^{-1}). It can be concluded that the catalyst has good stability and the leaching of Cu from the catalyst surface is low.

4. Conclusion

In summary, we demonstrate a Cu nanoparticle embedded and biguanidine modified Zr-UiO-66 MOF as a novel heterogeneous nanocomposite catalyst. A covalent post-synthetic modification approach was followed in this synthesis to immobilize the Cu NPs than the conventional deposition over the MOF. The strong chelating ability of biguanidine has been used to immobilize Cu NPs over it. The morphological structure was evaluated through different analytical methods. Thereafter, the nanocatalyst was explored in the Buchwald–Hartwig C–N and Ullmann type C–O cross coupling reactions for the synthesis of diverse range of diaryl amine and ethers under mild and green conditions affording outstanding yields. The material has been proved to be sufficiently rigid to be recycled for consecutive 11 cycles with only a slight decrease in activity after 8 runs.

Conflicts of interest

The authors declare that they have no known competing financial interests or personal relationships that could have appeared to influence the work reported in this paper.

Acknowledgements

We are thankful to Payame Noor University (PNU), Tehran, Iran for financial supports and Gobardanga Hindu College for providing research facilities.

References

1 H. Veisi, S. Hemmati and P. Safarimehr, *J. Catal.*, 2019, **365**, 204.
2 H. Veisi, M. Pirhayati and A. Kakanejadifard, *Tetrahedron Lett.*, 2017, **58**, 4269.
3 M. Kazemnejadi and A. R. Sardarian, *RSC Adv.*, 2016, **6**, 91999.
4 A. Dewaele, F. Verpoort and B. Sels, *ChemCatChem*, 2016, **8**, 3010.
5 H. Keypour, S. G. Saremi, H. Veisi and R. Azadbakht, *RSC Adv.*, 2016, **6**, 77020.
6 X. Qiu, S. Han, Y. Hu, M. Gao and H. Wang, *J. Mater. Chem. A*, 2014, **2**, 1493.
7 L. Chen, B. Li and D. Liu, *Catal. Lett.*, 2014, **144**, 1053.
8 M. Navidi, B. Movassagh and S. Rayati, *Appl. Organomet. Chem.*, 2013, **452**, 24.
9 V. Ganesan, M. Pal and M. Tiwari, *Bull. Mater. Sci.*, 2014, **37**, 623.
10 G. R. Reddy, S. Balasubramanian and K. Chennakesavulu, *J. Mater. Chem. A*, 2014, **2**, 15598.
11 S. Eyele-Mezui, E. Delahaye, G. Rogez and P. Rabu, *Eur. J. Inorg. Chem.*, 2012, **2012**, 5225.
12 S. Hemmati, M. Hekmati, D. Salamat, M. Yousefi, B. Karmakar and H. Veisi, *Polyhedron*, 2020, **179**, 114359.
13 N. C. Thacker, Z. Lin, T. Zhang, J. C. Gilhula, C. W. Abney and W. Lin, *J. Am. Chem. Soc.*, 2016, **138**, 3501.
14 A. Dhakshinamoorthy, A. M. Asiri and H. Garcia, *Chem. Commun.*, 2014, **50**, 12800.
15 W. J. Cui, G. Y. Zhang, T. L. Hu and X. H. Bu, *Coord. Chem. Rev.*, 2019, **387**, 79.
16 B. Gole, U. Sanyal, R. Banerjee and P. S. Mukherjee, *Inorg. Chem.*, 2016, **55**, 2345.
17 Y.-B. Huang, J. Liang, X.-S. Wang and R. Cao, *Chem. Soc. Rev.*, 2017, **46**, 126.
18 H. C. Zhou and S. Kitagawa, *Chem. Soc. Rev.*, 2014, **43**, 5415.
19 V. Pascanu, G. G. Miera, A. K. Inge and B. M. Matute, *J. Am. Chem. Soc.*, 2019, **141**, 7223.
20 Q. Yang, Q. Xu and H. L. Jiang, *Chem. Soc. Rev.*, 2017, **46**, 4774.
21 V. R. Bakuru, D. Davis and S. B. Kalidindi, *Dalton Trans.*, 2019, **48**, 8573.
22 M. Nasrabadi, M. A. Ghasemzadeh and M. R. Z. Monfared, *New J. Chem.*, 2019, **43**, 16033.
23 H. Lv, Y. Zhang, P. Chen, J. Xue, X. Jia and J. Chen, *Langmuir*, 2020, **36**, 4025.
24 Y.-Z. Chen and H.-L. Jiang, *Chem. Mater.*, 2016, **28**, 6698.
25 Y. Luan, H. Gao, R. S. Andriamitantsoa, N. Zheng and G. Wang, *J. Mater. Chem. A*, 2015, **3**, 17320.
26 H. Konnerth, B. M. Matsagar, S. S. Chen, M. H. G. Prechtl, F.-K. Shieh and K. C.-W. Wu, *Coord. Chem. Rev.*, 2020, **416**, 213319.
27 L. Zhu, X.-Q. Liu, H.-L. Jiang and L.-B. Sun, *Chem. Rev.*, 2017, **117**, 8129.
28 S. Koushik and S. Velmathi, *Chem.–Eur. J.*, 2019, **25**, 16451.
29 P. Li, S. Regati, H. C. Huang, H. D. Arman and B. L. Chen, *Chin. Chem. Lett.*, 2015, **26**, 6.
30 T. Tamoradi, H. Veisi and B. Karmakar, *ChemistrySelect*, 2019, **4**, 10953.
31 R. Ghorbani-Vaghei, H. Veisi, M. H. Aliani, P. Mohammadi and B. Karmakar, *J. Mol. Liq.*, 2021, **327**, 114868.
32 H. Veisi, S. Najafi and S. Hemmati, *Int. J. Biol. Macromol.*, 2018, **113**, 186.
33 H. Veisi, T. Tamoradi, A. Rashtiani, S. Hemmati and B. Karmakar, *J. Ind. Eng. Chem.*, 2020, **90**, 379.
34 S. Hemmati, M. M. Heravi, B. Karmakar and H. Veisi, *J. Mol. Liq.*, 2020, **319**, 114302.
35 H. Veisi, S. Azizi and P. Mohammadi, *J. Cleaner Prod.*, 2018, **170**, 1536.
36 H. Veisi, T. Tamoradi, B. Karmakar, P. Mohammadi and S. Hemmati, *Mater. Sci. Eng., C*, 2019, **104**, 109919.
37 T. Tamoradi, M. Daraie, M. M. Heravi and B. Karmakar, *New J. Chem.*, 2020, **44**, 11049.
38 H. Veisi, T. Tamoradi, B. Karmakar and S. Hemmati, *J. Phys. Chem. Solids*, 2020, **138**, 109256.
39 G. Evano, N. Blanchard and M. Toumi, *Chem. Rev.*, 2008, **108**, 3054.
40 J. P. Corbet and G. Mignani, *Chem. Rev.*, 2006, **106**, 2651.
41 L. Luza, A. Gual and J. Dupont, *ChemCatChem*, 2014, **6**, 702.
42 H. Weingarten, *J. Org. Chem.*, 1964, **29**, 3624.
43 J. C. Antilla, A. Klapars and S. L. Buchwald, *J. Am. Chem. Soc.*, 2002, **124**, 11684.
44 D. Toummini, A. Tlili, J. Berges, F. Ouazanni and M. Taillefer, *Chem.–Eur. J.*, 2014, **20**, 14619.
45 F. Monnier and M. Taillefer, *Angew. Chem., Int. Ed.*, 2008, **47**, 3096.
46 F. Monnier and M. Taillefer, *Angew. Chem., Int. Ed.*, 2009, **48**, 6954.
47 S. Bhunia, G. G. Pawar, S. Vijay Kumar, Y. Jiang and D. Ma, *Angew. Chem., Int. Ed.*, 2017, **56**, 16136.
48 S. Pradhan, P. B. De and T. Punniyamurthy, *J. Org. Chem.*, 2017, **82**, 4883.
49 M. Servalli, M. Ranocchiari and J. A. Van Bokhoven, *Chem. Commun.*, 2012, **48**, 1904–1906.
50 H. Veisi, Y. Metghalchi, M. Hekmati and S. Samadzadeh, *Appl. Organomet. Chem.*, 2017, **17**, 3676.
51 Y. Z. Huang, J. Gao, H. Ma, H. Miao and J. Xu, *Tetrahedron Lett.*, 2008, **49**, 948.
52 M. L. Kantam, R. Roy, S. Roy, B. Sreedhar and R. L. De, *Catal. Commun.*, 2008, **9**, 2226.
53 N. R. Jogdand, B. B. Shingate and M. S. Shingare, *Tetrahedron Lett.*, 2009, **50**, 4019.
54 S. Jammi, S. Sakthivel, L. Rout, T. Mukherjee, S. Mandal, R. Mitra, P. Saha and T. Punniyamurthy, *J. Org. Chem.*, 2009, **74**, 1971.

55 R. Ghorbani-Vaghei, S. Hemmati and H. Veisi, *Tetrahedron Lett.*, 2013, **54**, 7095.
56 J. B. Zhu, L. Cheng, Y. Zhang, R. G. Xie and J. S. You, *J. Org. Chem.*, 2007, **72**, 2737.
57 M. Akhavan, S. Hemmati, M. Hekmati and H. Veisi, *New J. Chem.*, 2018, **42**, 2782.
58 M. Tao and W. Lei, *Tetrahedron Lett.*, 2007, **48**, 95.
59 S. M. Islam, S. Mondal, P. Mondal, S. Singh Roy, K. Tuhina, N. Salam and M. Mobarak, *J. Organomet. Chem.*, 2012, **696**, 4264.
60 H. Veisi, M. Hamelian, S. Hemmati and A. Dalvand, *Tetrahedron Lett.*, 2017, **58**, 4440.